Photoinduced light absorption and dichroism of $Ca_3Mn_2Ge_3O_{12}$ garnet as a probe of electronic processes and intrinsic electric fields

V. V. Eremenko, S. L. Gnatchenko, I. S. Kachur, V. G. Piryatinskaya, A. M. Ratner, and V. V. Shapiro

B. Verkin Institute for Low Temperature Physics and Engineering, National Academy of Sciences of Ukraine
47 Lenin Ave., 61164 Kharkov, Ukraine
E-mail: piryatinskaya@ilt.kharkov.ua

M. Fally and R. A. Rupp

Institute of Experimental Physics, Vienna University, A-1090 Vienna, Strudlhofgasse 4, Austria

Measurements of photoinduced light absorption in $Ca_3Mn_2Ge_3O_{12}$ revealed some unusual features: a saturation with the pumping intensity and a broad straggling of relaxation times with a predominance of very long times. These experimental facts cannot be understood in terms of photoinduced absorption centers associated with impurities or lattice defects, but are naturally explained within the notion of random electric fields of active charges. Active charges are produced by light pumping via the dissociation of coupled pairs of charges (consisting of a Mn-hole coupled with a compensating negative impurity or a negatively charged vacancy) which exist in the ground state. Such active charges create electric fields in a larger volume than coupled pairs, thus enhancing the probability for forbidden optical transitions. On the other hand, the random fields of active charges promote hopping of holes and hence the relaxation of photoinduced effects. A broad distribution of the magnitudes of random fields gives rise to a very broad range of the hole hopping rates. There is also a much faster annihilation process immediately conditioned by light pumping. The simultaneous action of these relaxation channels, depending on the number of active charges, pumping intensity and temperature, explains the entire experimental picture qualitatively and in part quantitatively. Photoinduced dichroism as well as birefringence, observed under polarized pumping, are caused by an anisotropic distribution of photoproduced holes over polarization directions.

PACS: **78.40.−q**

Introduction

There exists a class of related long-lived photoinduced phenomena in magnetic insulators conventionally associated with transfer of charges caused by photoillumination. Such phenomena are usually observed in ferromagnets or ferrimagnets within the region of magnetic ordering, i.e., the Curie temperature exceeds the upper temperature boundary of the existence of long-lived photoinduced phenomena. In this temperature region, interrelated photoinduced changes in optical and magnetic properties take place. For instance, in the case of yttrium iron garnet, $Y_3Fe_5O_{12}$, illumination with linearly polarized light induces a change of magnetic anisotropy [1−3], linear dichroism [3], and domain structure [4]. Unpolarized light affects the magnetic permeability and susceptibility [5,6], coercivity and mobility of domain walls [7,8], magnetostriction [9], and optical absorption [10,11]. The interconnected variations in optical and magnetic properties make up a complicate physical picture. This has hampered the exploration of the detailed nature of long-lived photoinduced changes.

The purpose of the present work is to elucidate the mechanism of long-lived photoinduced changes in magnetic insulators, in particular, the charge transfer process under photoillumination and the subsequent relaxation in the absence of illumination.

To that end, it is necessary to separate the persistent photoinduced changes of optical properties from those of magnetic characteristics related to a magnetically ordered state. Antiferromagnetic garnets with a low Néel temperature T_N offer this possibility because they exhibit a broad temperature range between T_N and the temperature limit for the existence of long-lived photoinduced phenomena. Keeping this in mind, the garnet $Ca_3Mn_2Ge_3O_{12}$, with the Néel temperature $T_N = 13.85$ K, was chosen as a favorable object of investigation.

The elucidation of the mechanism of photoinduced processes is facilitated by the results of the preceding investigation of this crystal carried out by the authors. Recently it was shown [12] that illumination of the garnet $Ca_3Mn_2Ge_3O_{12}$ with visible unpolarized light ($\lambda = 633$ nm) causes a noticeable increase (up to 15%) of the optical absorption coefficient at the same wavelength. Illumination of this crystal with linearly polarized light results in the appearance of linear birefringence which is caused by an anisotropic spatial redistribution of charges [13–16]. Electrons are transferred from Mn^{3+} ions, occupying regular positions in the lattice, to Mn^{4+} ions, which are present in the crystal in a small concentration due to a weak impurity of negative charges. The redistribution of charges between orientationally nonequivalent octahedral positions lowers the crystal symmetry and gives rise to birefringence. As will be shown below, the same mechanism is responsible for linear dichroism.

Thus the photoinduced phenomena in the garnet $Ca_3Mn_2Ge_3O_{12}$ can be divided into two groups: those induced only by linearly polarized light (photoinduced birefringence and linear dichroism) and phenomena induced by light irrespective of its polarization properties (photoinduced absorption).

The paper is organized as follows: we start with the basic assumptions, the statement of the problem, and some general remarks. Then, we analyze the problem and draw some general conclusions about photoinduced changes by transfer of charges, which will be helpful in the discussion that follows. The experimental studies of photoinduced absorption, described in Sec. 3, verify these conclusions and reveal the detailed physical picture. In the subsequent Sections, these experimental data are interpreted quantitatively in order to discover the peculiarities of the photoinduced processes and the physically relevant parameters.

1. Basic assumptions and statement of the problem

It is well established that photoinduced changes of the optical properties are conditioned by the transfer of charges (displacement of holes or electrons) between lattice ions [17,18]. In the case of the garnet $Ca_3Mn_2Ge_3O_{12}$, Mn-holes are transferred by light in the Mn sublattice (between Mn^{4+} and Mn^{3+} ions) [12–16]. The concentration of Mn^{4+} is low and corresponds to that of negative impurities or negatively charged Ge vacancies [19,20]. Prior to the description of our experiment, let us outline some basic model assumptions which will be helpful for the analysis of the experimental results (for simplicity, impurity centers with negative unit charge are considered below).

(*i*) *Ground state.* In the ground state of the crystal, each Mn^{4+} ion is separated from a negatively charged impurity by the minimal possible distance, which does not exceed the lattice period. Thus, in the ground state the positive effective charges (the Mn^{4+} ions) and the negative impurity charges form coupled pairs. They are inactive in the sense that their electric field acts only on a negligible volume fraction of the crystal if compared with that of separated charges of opposite sign.

(*ii*) *Creation of active charges under illumination.* The binding of a coupled pair is too strong for the pair to be thermally dissociated. However, it can be dissociated by light. Thereby an electron is taken away from a regular Mn^{3+} ion (positioned far from the coupled pair) and transferred to the Mn^{4+} component of a coupled pair (as shown by the thin arrow in Fig. 1). This results in the creation of active charges: a Mn^{4+} ion and a negative impurity charge that are spatially separated from each other. Note that the free electrons produced can also recombine (and with a greater probability) with any of the existing active charges (separated Mn^{4+} ions). This relaxation channel is indicated by the bold arrow in Fig. 1.

(*iii*) *The achievable fraction of dissociated active charges is much less than unity.* The photoinduced increase of the number of active charges (the channel designated by the thin arrow in Fig. 1) is possible provided that this channel is not compensated completely by the channel of destruction of existing active charges (shown by the bold arrow). This condition is met only if the number of active charges is much less than the number of coupled pairs, since the cross section for trapping of electrons is much larger for a separate Mn^{4+} ion than for the Mn^{4+} component of a coupled pair.

Mn³⁺ (regular site) — Mn^{3+} (regular site)

Mn^{4+} (hole)

hole to be formed by electron transfer

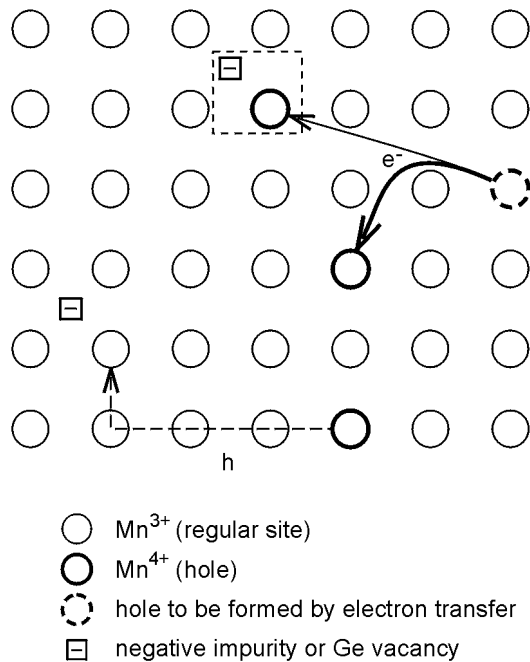negative impurity or Ge vacancy

Fig. 1. Scheme of photoproduction and relaxation of active charges. An active charge is generated through the transfer of an electron from a regular Mn^{3+} ion to the Mn^{4+} component of a coupled pair (thin solid arrow). The same electron, being transferred to an existing active charge, annihilates it (bold solid arrow). The dashed arrow shows the relaxation of an active charge through the hopping of a hole and formation of a coupled pair.

(*iv*) *Existence of two relaxation times for active charges.* Photoproduced active charges relax in two different ways: First, through recombination with photoproduced electrons (the process shown by the bold arrow in Fig. 1). The characteristic time τ_p of this process is inversely proportional to the pumping intensity I,

$$\tau_p = C/I \tag{1}$$

and is mainly independent of temperature.

Second, an active charge (hole at Mn^{4+}) can disappear by forming an inactive coupled pair with a separate negative impurity ion (or a germanium vacancy). This process is preceded by a diffusive motion of a hole, bringing it into a close vicinity of the negative ion (as shown by the dashed line in Fig. 1). The characteristic time of such a diffusion process is denoted by τ_{dif}. It generally exceeds τ_p and decreases with rising temperature.

2. Experiment

2.1. Experimental setup

For the measurements of photoinduced absorption and linear dichroism, the samples were prepared in the form of plane-parallel plates of thickness $d \approx 35$ μm. The samples were cut from a single crystal of calcium-manganese-germanium garnet (CaMnGeG), were polished mechanically and then annealed at the temperature $T \approx 1000°C$ to eliminate internal stresses caused by polishing.

The measurements of photoinduced absorption were performed with allowance for a twin domain structure of CaMnGeG [21–23]. It arises below the temperature of 520 K due to a Jahn–Teller phase transition from the cubic to the tetragonal phase. A special thermal treatment [22] of the samples was carried out to increase the average size of the domains up to about 1 mm. A special sample holder with a diaphragm was used to select a single-domain region of the sample having its tetragonal axis perpendicular to the surface of the plate. Thus the results of the measurements refer to a sample with the tetragonal axis perpendicular to the surface. The sample was placed in a helium cryostat where the temperature could be continuously varied from 2 K to 300 K. The sample temperature was measured using a copper–constantan thermocouple.

The effect of illumination on the optical absorption and linear dichroism of CaMnGeG was studied with the use of an optical setup with two light sources. A helium–neon laser with an output power of about $2·10^{-3}$ W and a wavelength of $\lambda = 633$ nm was used as the pumping source. The laser light had no fixed direction of polarization. The stable wideband emission of an arc xenon lamp, dispersed by a prism monochromator (with the linear dispersion of 12 nm/mm at $\lambda = 500$ nm), was used as probe light. The intensity of the probe beam has been chosen sufficiently low as not to cause any photoinduced phenomena.

The setup for measuring the time dependence of the linear dichroism is shown schematically in Fig. 2. The characteristic feature of this setup is the following: after passing through the sample, the intensities of two light beams, linearly polarized in mutually perpendicular directions, are in turn measured by the same channel of the registration system. This method enables us to measure the dichroism of the sample, expressed as the difference in the absorption of perpendicularly polarized rays, with minimal errors.

The arc lamp (*1*) and the monochromator (*3*) form the probe beam with the wavelength
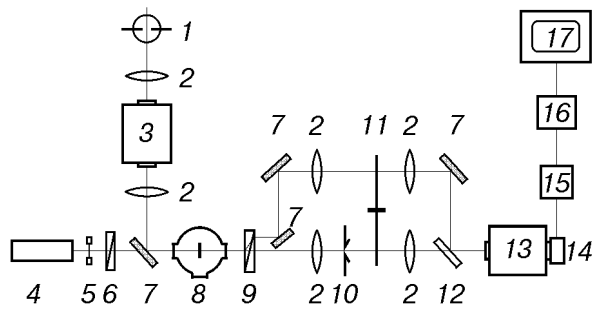
Fig. 2. Diagram of the setup for measuring photoinduced absorption and dichroism. *1* — arc lamp; *2* — lens; *3* — input monochromator; *4* — helium–neon laser; *5* — shutter; *6* — polarizer (Glan prism); *7* — mirror; *8* — cryostat with the sample; *9* — polarizer (Rochon prism); *10* — a variable slit; *11* — rotating disk; *12* — quartz plate; *13* — monochromator; *14* — photomultiplier; *15* — amplifier; *16* — analog–digital transformer; *17* — computer.

$\lambda = 565$ nm. This beam passes through the sample (*8*) parallel to the tetragonal axis of the crystal. After passing through the polarizer (*9*), the probe beam is split into two mutually perpendicularly polarized beams which are spatially separated from each other. Before irradiating the sample, the intensities of these beams are made exactly equal by using a slit (*10*). The rotating disk (*11*) opens the path for the beams for the same time intervals (30 s) alternately. Then the beams pass through the second monochromator (*13*) and are finally registered by the photomultiplier (*14*). The signal of the photomultiplier is enhanced by a direct-current amplifier (*15*), then transformed by an analog-digital converter (*16*) to consecutive codes which are transferred for accumulation to a computer (*17*). The accumulation time of the signal was 1 s (its minimal value being 0.1 s).

The pumping beam from the laser (*4*) is slightly deflected from the optical axis in a direction perpendicular to the plane of the figure; it passes through the polarizer (*6*) over the mirror (*7*) and hits the sample. After passing through the cryostat (*8*), the pumping beam is blocked by a diaphragm. The scattered pumping light is cut off from the photomultiplier (*14*) by the second monochromator (*13*) tuned to the wavelength of probe light.

The setup was used for measurements in three regimes:

(*i*) Measurement of the absorption spectrum for unpolarized light before or after irradiation of the sample, the laser (*4*) being switched off during measurement. In that configuration, both the polarizers (*6*) and (*9*), as well as the monochromator (*13*), are removed. Using the monochromator (*3*), the wavelength of the probe light was scanned within the examined region and synchronously transferred to the computer. The optical absorption spectrum was obtained from the measurements by the usual processing of the transmission and reflection spectra.

It was established that the transmission of the CaMnGeG sample was noticeably decreased by illumination, whereas no photoinduced variation in the reflection coefficient was registered within the interval 500 nm $< \lambda <$ 800 nm. Thus the decrease in transmission observed in this spectral region should be assigned to the light-induced augmentation of the optical absorption coefficient, defined as follows:

$$\Delta K = d^{-1} \ln (j_0 / j) . \qquad (2)$$

Here j_0 and j are the intensities of the transmitted probe beam before and after illumination, respectively.

(*ii*) Measurement of the photoinduced absorption for unpolarized light with a fixed wavelength ($\lambda = 565$ nm) during irradiation of the sample with unpolarized light ($\lambda = 633$ nm). Such measurements were carried out similarly to Item (*i*) but using both the monochromators (*3*) and (*13*) tuned to the same fixed wavelength $\lambda = 565$ nm.

(*iii*) Measurement of photoinduced dichroism at a fixed wavelength ($\lambda = 565$ nm) during irradiation of the sample with linearly polarized light ($\lambda = 633$ nm). The probe light passes through the sample along its tetragonal axis [001] and is split into two beams polarized in the mutually perpendicular directions [110] and [$\bar{1}$10] by the polarizer (*9*). Those polarization directions correspond to maximal dichroism. The pumping beam passes through the sample parallel to the same axis [001], its polarization being determined by the polarizer (*6*). For definiteness, let the pumping light be polarized in the direction [110]. Then the photoinduced augmentations of the absorption coefficient, derived from Eq. (2), are denoted by $\Delta K_{\parallel}$ and $\Delta K_{\perp}$ for the probe beams polarized in the directions [110] and [$\bar{1}$10], respectively. The photoinduced dichroism ΔK_d is defined as

$$\Delta K_d = \Delta K_{\perp} - \Delta K_{\parallel} . \qquad (3)$$

2.2. Experimental results: Photoinduced absorption

Prior to studying photoinduced changes of the absorption, the absorption spectrum of CaMnGeG was measured within the spectral interval 540 nm $<$
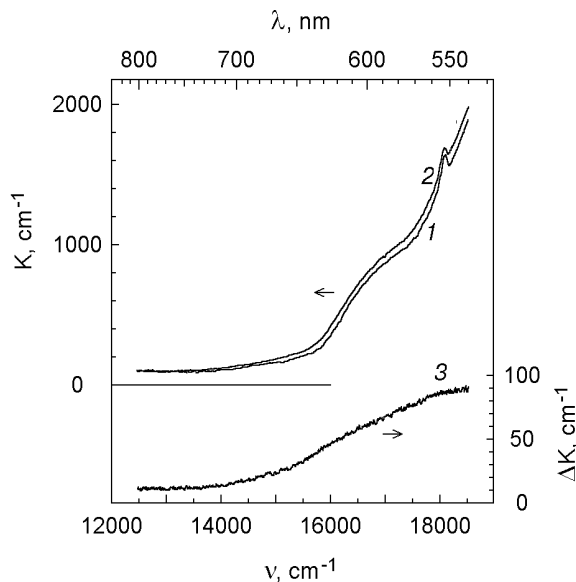
Fig. 3. Spectral dependence of the optical absorption coefficient before illumination (*1*) and after illumination (*2*) measured for the $Ca_3Mn_2Ge_3O_{12}$ garnet in the wavelength interval 540 to 800 nm at the temperature $T = 23$ K. Curve *3* shows the photoinduced augmentation of the absorption coefficient, defined as the difference of the curves *2* and *1*.

Fig. 4. Time dependences of the light-induced addition, ΔK, to the optical absorption coefficient of the garnet $Ca_3Mn_2Ge_3O_{12}$ measured at the wavelength 565 nm and $T = 23$ K under laser irradiation with different intensities i (given in units of the maximal pumping intensity): 1 (*1*); 0.24 (*2*); 0.085 (*3*); 0.05 (*4*). Experimental data are plotted by dots; solid lines show the solution of the kinetic equation (31).

$< \lambda < 800$ nm. The result is shown in Fig. 3 (curve *1*). As can be seen, the garnet is relatively transparent in the interval 650 nm $< \lambda <$800 nm, but its optical absorption strongly increases with decreasing wavelength in the range $\lambda < 650$ nm. For $\lambda < 540$ nm, the transmission of the crystal becomes very low, thus limiting the measurement of the spectrum on the high-frequency side.

Such a spectral dependence of the absorption, strongly increasing with decreasing wavelength below 650 nm, can be attributed to the wide band with a maximum near 500 nm which is usually present in the optical spectra of compounds with Mn^{3+} and is related to the optical transition $^5E_g \rightarrow {}^5T_{2g}$ in the Mn^{3+} ion [24,25]. In the case of CaMnGeG, where a Mn^{3+} ion occupies an octahedral position, its orbitally degenerate states ^5E_g and $^5T_{2g}$ are split by the tetragonal distortion of oxygen octahedrons caused by the Jahn–Teller effect [21]. However, the splitting components of both states retain their g symmetry, so that the optical transition $^5E_g \rightarrow {}^5T_{2g}$ is forbidden in the dipole approximation. This reduces the absorption coefficient by four orders of magnitude as compared to an allowed transition.

In Fig. 3 (curve *2*) the spectral dependence of the absorption coefficient after irradiation with unpolarized light is shown, while the lower curve *3* displays the photoinduced change of the absorption
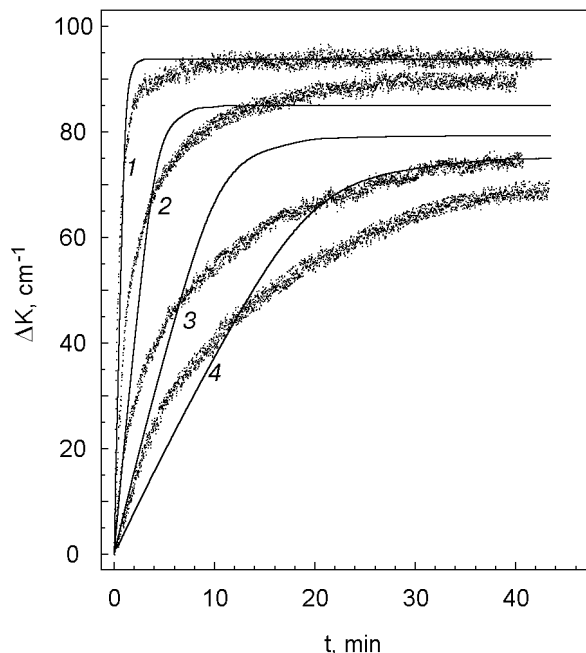
coefficient obtained by subtracting curve *1* from curve *2*. It can be seen that the absorption coefficient and its photoinduced part have similar spectral dependences. This allows one to conclude that the initial absorption and its photoinduced augmentation are related to the same optical transition. This is the fundamental inference underlying the suggested model and will be corroborated by the further analysis.

Figure 4 demonstrates the observed time dependences of the photoinduced addition, $\Delta K(t)$, to the absorption coefficient at the wavelength 565 nm under irradiation with different pumping intensities i. It can be seen that the photoinduced absorption saturates with time. The time t_{sat}, during which $\Delta K(t)$ achieves 90% of the saturation level $\Delta K(\infty)$, decreases with an increase of the pumping intensity i approximately as i^{-1}. However, the level of saturation $\Delta K(\infty)$ itself has a much weaker dependence on i and varies only by 25% as i changes by a factor of twenty. This agrees with the statement given in Item (*iv*) of Sec. 1. Indeed, the saturation time t_{sat} practically coincides with the lifetime of photoproduced active charges (their lifetime is equal to the smaller of the times τ_p and τ_{dif}). The latter, as will be shown below, is very large at low tempera-
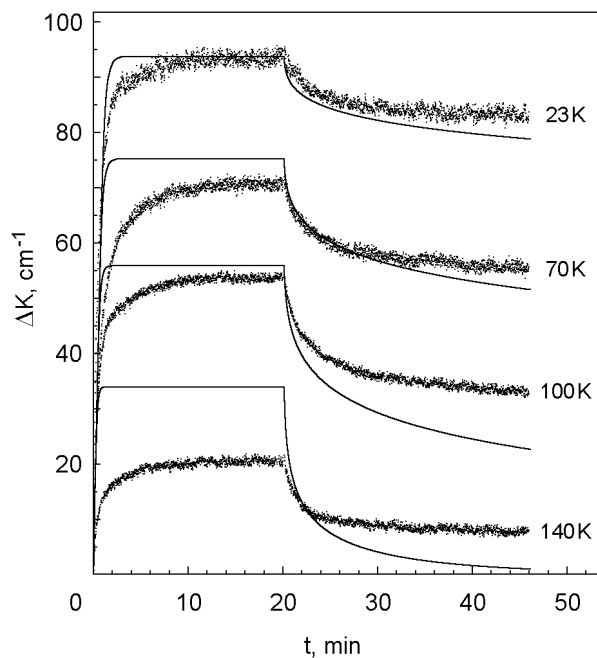
Fig. 5. Time dependences of the light-induced addition, ΔK, to the absorption coefficient measured at the wavelength 565 nm and different temperatures under the maximal pumping intensity ($i = 1$). Pumping was switched off at the time $t = 20$ min. Experimental data are plotted by dots; the solid lines show the solution of the kinetic equation (31).

tures, so that t_{sat} mainly coincides with the time τ_p proportional to i^{-1}. As to the saturation level $\Delta K(\infty)$, it is mainly determined by pumping intensity i multiplied by t_{sat}; this product is almost independent of i. This qualitatively explains the observed weak dependence of the saturation level on pumping intensity.

The saturation value of photoinduced absorption decreases with increasing temperature. This can be seen from Fig. 5, where the time dependences $\Delta K(t)$ at different temperatures are presented. The curves were measured for $\lambda = 565$ nm and $i = 1$ (maximal pumping in relative units). The decrease of the saturation level with increasing temperature is caused by a decrease of the relaxation time τ_{dif} down to a value comparable with τ_p (see Sec. 1, Item (iv)), so that the resulting relaxation time diminishes. Note that light-induced absorption in CaMnGeG is no longer observed when the sample temperature exceeds 190 K.

In order to explore the relaxation of photoinduced absorption, the time dependences of ΔK were measured upon switching off the pumping light. The corresponding relaxation curves are shown in Fig. 5 for the maximal pumping and different temperatures. Attention should be paid to the fact that each of these curves displays the existence of relaxa-

tion components with strongly differing values of the time constant τ. For a fast component, distinctly seen in Fig. 5 just after the switching off of the irradiation, τ does not exceed a few minutes. A very small slope of the relaxation curves, observed 25 min after the switching off of the illumination, proves the existence of a practically stable component with a τ exceeding several hours. As will be shown in Sec. 3, the interval between these limiting values for τ is continuously filled in by intermediate relaxation components. At low temperatures, a predominant part of photoinduced absorption (about 90%) is produced by long-lived centers with lifetime τ exceeding the time τ_p at least by two orders of magnitude.

Note that the shape of the relaxation curve (Fig. 5) cannot be explained by the dependence of the relaxation time on the number of active charges, which decreases in the course of relaxation. Indeed, as is seen from Fig. 6, the shape of the relaxation curve is practically independent of the achieved level of photoinduced absorption, no matter how it is changed: by varying the intensity or duration of the pumping.

Thus there exists a practically stable residual contribution ΔK_{stab} to the photoinduced absorption. At 23 K, ΔK_{stab} amounts to about 90% of the initial ΔK value. As can be seen from Fig. 7, with rising
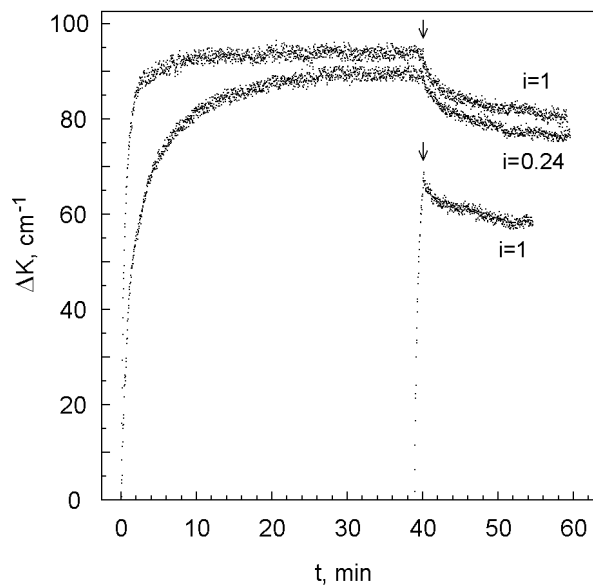

Fig. 6. Comparison of the relaxation curves of the photoinduced absorption after the moment of switching off of the illumination (indicated by an arrow), preceded by various ways of pumping: long pumping until saturation (two upper curves) and short pumping far from saturation (lower curve). The pumping intensity is shown in the figure. The measurements were performed at $\lambda = 565$ nm and $T = 23$ K (the moments of the onset of pumping are indicated arbitrarily).
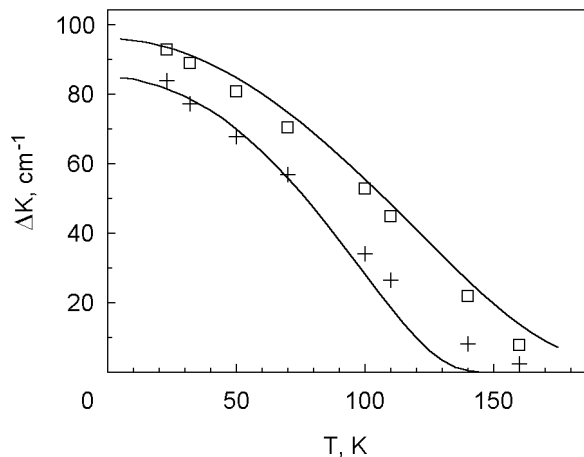
Fig. 7. Temperature dependences of the saturation level of the photoinduced absorption (upper curve) and of its stable part, defined as the ordinate of the corresponding relaxation curve after 25 min upon the switching off of the irradiation (lower curve). Squares and crosses denote experimental points; solid lines show the solution of the kinetic equation (31).

Fig. 8. Spectral dependences of the photoinduced addition to the absorption coefficient for the pumping light polarization [110] and the probe light polarizations [110] and [$\bar{1}$10] ($\Delta K_{\parallel}$ and $\Delta K_{\perp}$, respectively) (*a*). Spectral dependence of the linear dichroism, defined as the difference of the above curves $\Delta K_{\perp} - \Delta K_{\parallel}$ (*b*). The measurements pertain to $T = 35$ K and $\lambda = 565$ nm.

temperature both the quantity ΔK_{stab} and its ratio to the saturation level decrease fast and monotonically. This points to a strong thermal acceleration of the relaxation of active charges, related to a decrease of τ_{dif}.

2.3. Experimental results: Photoinduced dichroism

Figure 8 presents the spectrum of photoinduced dichroism, measured under pumping with linearly polarized light, together with the photoinduced absorption spectra measured with the probe light polarized parallel and perpendicular relative to pumping. The similiarity of all three spectra provides evidence that photoinduced dichroism and absorption are due to the same optical centers and to closely interconnected mechanisms. This conclusion is corroborated by the practical coincidence of the relaxation kinetics measured for dichroism and absorption after the switching off of the irradiation (Figs. 5,9,10).

However, the temperature dependences of the saturation level, measured under pumping for dichroism and absorption, differ somewhat in their character, as can be seen from a comparison of Figs. 7 and 11. The photoinduced dichroism (Fig. 11) depends only very weakly on temperature up to 100 K, whereas the photoinduced absorption (Fig. 7) diminishes in the same temperature interval by 40%. This is an indication of certain differences in the relaxation mechanisms, which will be analyzed below (Sec. 6).
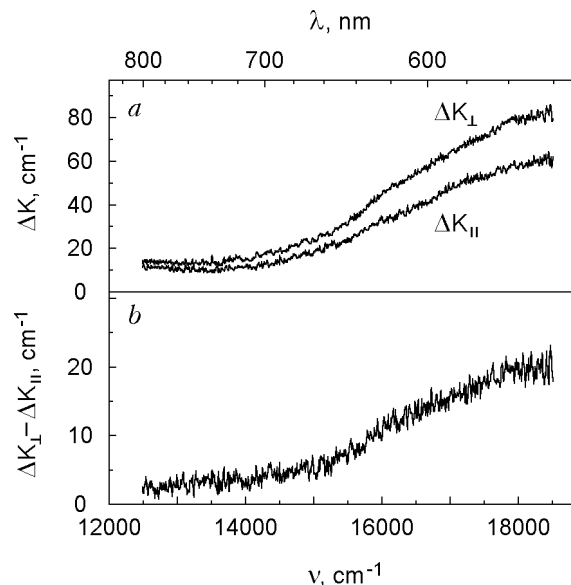
For comparison, the corresponding data on photoinduced birefringence [14,15] are plotted in Figs. 10 and 11. The photoinduced dichroism and
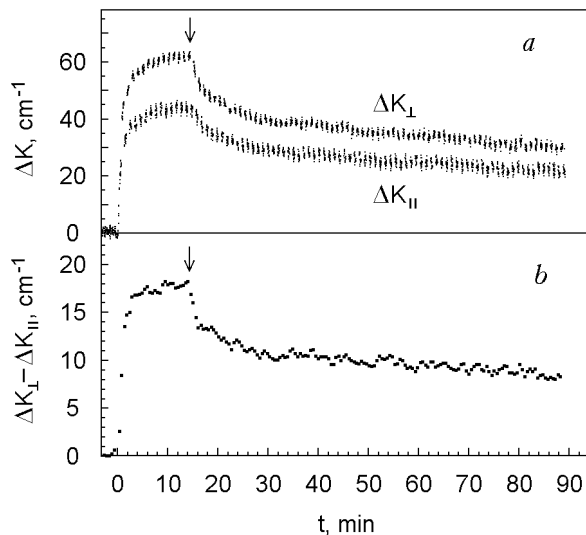

Fig. 9. Time dependences of the photoinduced addition to the absorption coefficient for the pumping light polarization [110] and the probe light polarizations [110] and [$\bar{1}$10] ($\Delta K_{\parallel}$ and $\Delta K_{\perp}$, respectively) (*a*). Time dependence of the linear dichroism, defined as the difference of the above curves $\Delta K_{\perp} - \Delta K_{\parallel}$ (*b*). The measurements are related to $T = 90$ K and $\lambda = 565$ nm. The moment of the switching off of the illumination is indicated by an arrow.
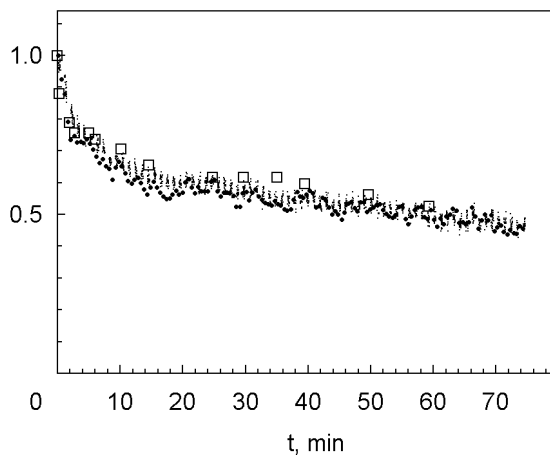
Fig. 10. Time dependences of the photoinduced absorption (dots) and dichroism (full circles) measured at $T = 90$ K and $\lambda = 565$ nm after the moment of the switching off of the irradiation, $t = 0$. For comparison, the time dependence of the photoinduced birefringence [15] is plotted by the squares. All curves are normalized to unity at $t = 0$.

Fig. 12. Time dependence of $\Delta K_\perp$ and $\Delta K_\parallel$ (*a*) and of the photoinduced dichroism $\Delta K_\perp - \Delta K_\parallel$ (*b*) measured at $T = 90$ K under varying conditions of pumping. At the moment *1* (indicated by arrow), the direction of the pumping polarization was turned by 90°; at the moment *2*, the polarized pumping was changed to unpolarized one.

birefringence display a complete similarity in their time and temperature behavior.

Similarly to the photoinduced birefringence, the photoinduced dichroism can be eliminated by unpolarized light (Fig. 12). Note that the time, required for the complete elimination of photoinduced dichroism (about 4 min), coincides with the time for achieving the saturation level. If the direction of pumping polarization is changed by $\pi/2$, then the photoinduced dichroism is correspondingly rewritten during the same time interval of 4 min (Fig. 12).

The above-stated complete similarity between photoinduced dichroism and birefringence provides
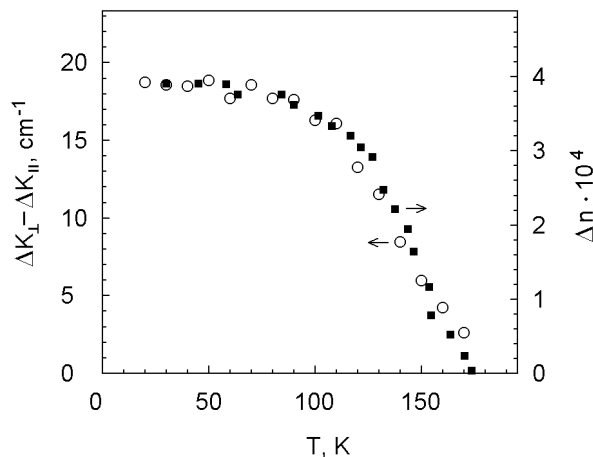

Fig. 11. Saturation values of the photoinduced dichroism (circles, left scale) and birefringence [14] (squares, right scale) measured versus temperature.
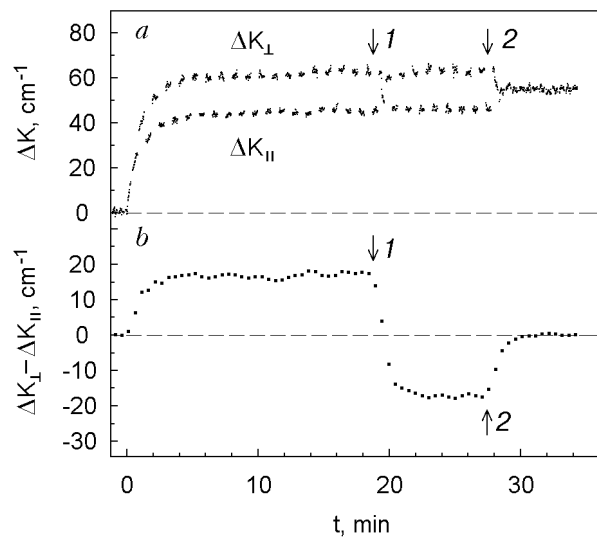
evidence for a common nature of these phenomena, which will be considered in Sec. 6.

3. Nature of the photoinduced absorption

All experimental findings will be used for the reconstruction of the corresponding electronic processes. This problem will be solved below in two steps. At first, the mechanism of photoinduced absorption will be established on the basis of its experimental dependences on pumping intensity, time, and temperature. Then the experimental data on dichroism will be used to derive some essential details of this mechanism.

The model of photoinduced absorption, which has to be developed on the basis of the experiments, must explain the broad distribution of photoinduced absorption centers over relaxation times. To clarify the mechanism of photoinduced absorption, two alternatives could be considered:

(a) The photoinduced absorption is caused by some new absorption centers produced by photoillumination of the crystal. They are different from the Mn^{3+} ions responsible for the usual absorption in the absence of illumination and, hence, can be related to some impurities or lattice defects.

(b) The photoinduced absorption is associated with the same Mn^{3+} ions that are responsible for absorption in the absence of illumination. Under irradiation, this absorption is enhanced by active charges which partially lift (mainly by their electric

fields) the forbiddenness of the $^5E_g \to {}^5T_{2g}$ optical transition in Mn^{3+} ions. On the other hand, the electric fields of the active charges strongly affect their lifetime, resulting in their broad distribution over lifetimes. Such a pattern is suggested by the similiarity of the spectral dependences of the initial absorption and its photoinduced augmentation.

The model (a) should be discarded for the following reason. The photoinduced absorption centers responsible for the observed relaxation scenario (Fig. 5) must have different relaxation times τ_1, τ_2, ..., the shortest of which being less than 2 min and the longest amounting to at least several hours. As temperature rises, the times τ_j strongly shorten (which follows from the diminution of the photoinduced absorption), whereas the shape of the relaxation curve varies rather weakly, and the stable part of the photoinduced absorption decreases monotonically (Fig. 7). This means that with increasing temperature all relaxation components move to the left along the τ axis with nearly the same rates, each of them being replaced by the nearest component with a longer τ. Such a scenario implies the existence of a large number of relaxation components with regular distribution on the τ axis and with an approximate coincidence of their activation energies. For relaxation components, associated with impurity or defect centers, this is highly improbable.

The exact meaning of this statement can be expressed in terms of a kinetic equation written under the assumption (a). Taking into account a broad lifetime distribution of photoinduced absorption centers (see Fig. 5), we classify them by their lifetimes τ_j in the excited state. The number $n_j(T, t)$ of excited centers of the jth type is described by the kinetic equation

$$\partial n_j(T, t)/\partial t = I_j \, (n_{0j} - n_j) - n_j \Gamma_j(T) \, . \qquad (4)$$

Here n_{0j} is the total number of centers of the jth type; n_j or $n_{0j} - n_j$ is their number in the excited or ground state, respectively; I_j stands for their pumping rate; $\Gamma_j = 1/\tau_j$ is relaxation rate, and T is the temperature. The excited centers of the jth type make a contribution $\alpha_j n_j$ to the photoinduced absorption. Equation (4) is easily solved in the relaxation regime after the switching off of the irradiation. As the initial condition, we use the stationary solution of Eq. (4) under pumping in the regime of saturation. Finally, the photoinduced augmentation to the absorption coefficient takes on the form

$$\Delta K(T, t) = \sum_j \alpha_j n_j(t) =$$

$$= \sum_j \left\{ \alpha_j n_{0j} / [1 + \gamma_j(T)] \right\} \exp \left\{ - t\Gamma_j(T) \right\} \qquad (5)$$

with $\gamma_j = \Gamma_j(T)/I_j$ (the time t is counted from the moment where the illumination is switched off).

Let us separate from the sum (5) a practically stable photoinduced contribution to the absorption, $\Delta K_{stab}(T)$, related to relaxation components with very low relaxation rates $\Gamma_j < \Gamma_{stab} \lesssim (300 \text{ min})^{-1}$:

$$\Delta K_{stab}(T) = \sum{}' \alpha_j n_{0j} \, . \qquad (6)$$

Here the summation goes over indices j for which $\Gamma_j(T) < \Gamma_{stab}$, the summands $\alpha_j n_{0j}$ not depending on temperature.

With rising temperature the sum (6) diminishes due to a decrease in the number of summands for which $\Gamma_j(T)$ remains less than Γ_{stab}. To fit Eq. (6) with the monotonic temperature dependence $\Delta K_{stab}(T)$ shown in Fig. 7, it is necessary to assume that each of the sequences $n_{0j}\alpha_j$ and $\Gamma_j(T)$ is of regular character and that the latter retains its character in a broad temperature range where the quantities $\Gamma_j(T)$ vary considerably. Since it is very improbable that such relaxation components originate from the presence of a variety of impurity centers, it is more plausible to suggest the existence of some identical active centers relaxing under different conditions. Such a mechanism is developed below.

4. Photoinduced absorption: Model of forbidden optical transitions enhanced by random electric fields

4.1. Random fields, their role, and the distribution over magnitudes

The model of random electric fields is based on the well-established fact of the presence of Mn^{4+} ions in the $Ca_3Mn_2Ge_3O_{12}$ garnet [19,20]. An estimation shows that the electric field of these ions, which are contained in a concentration of a few hundredths of an atomic percent, is sufficient to noticeably enhance the probability of the forbidden optical transition $^5E_g \to {}^5T_{2g}$ between even Mn^{3+} states (because the electric field produces an odd addition to an even state). The model of random electric fields consists in the following.

Since the crystal as a whole must be electrically neutral, it contains negative impurity ions or cation vacancies (for brevity we will speak about impurity ions with unit effective charge). The concentration of these impurities coincides with that of Mn^{4+} ions. The electrostatic energy is minimized if the excess positive charges, i.e., Mn-holes, occupy positions

adjacent to negative impurity charges in the Mn^{3+} sublattice. Hence, in the ground state all charges form coupled pairs, i.e., dipoles with a length of a few angstroms. Under photoillumination, some electrons are transferred from regular Mn^{3+} ions to Mn^{4+} ions coupled with such negative impurities, thus creating pairs of spatially separated charges of opposite signs (as shown in Fig. 1). These active charges produce electric fields extending into a larger space than coupled pairs and therefore enhance the probability for the forbidden optical transition. At low concentrations N of active charges, the photoinduced absorption is proportional to N.

On the other hand, the random electric fields of active charges promote hops of holes between Mn ions, which accelerates their recombination with negative impurity charges (for brevity, we use the term recombination as a synonym for the formation of an inactive coupled pair from an active charge and a negative impurity ion). The hopping probability, which determines the lifetime of the active charges, depends on the magnitude of the random electric field. Below we will consider their distribution over magnitudes (Sec. 4.1), the corresponding lifetime of active charges (Sec. 4.2), and their kinetics (Sec. 4.3, 4.4).

Active charges (numbered by the subscript i) create at a fixed point A random fields $\mathbf{F}_i$ which are assumed to be statistically independent. The squared total field per unit volume at the point A, averaged over random positions of charges, is estimated by

$$\langle \mathbf{F}^2 \rangle \equiv 3 \langle F_x^2 \rangle = \sum_i \langle F_i^2 \rangle = \int_{\beta N^{-1/3}}^{\infty} (e/\varepsilon r^2)^2 N 4\pi r^2 dr =$$

$$= 4\pi N^{4/3} (e^2/\varepsilon^2 \beta) . \qquad (7)$$

Here x, y, z are the equivalent Cartesian axes; N is the number of active charges per unit volume; β is a numerical constant defined below; e stands for the unit charge, and $\varepsilon \approx 3\varepsilon_0/(2 + \varepsilon_0) \approx 2$ is the effective permittivity (ε_0 is the static permittivity of the crystal). The integration in (7) is carried out over the distance r of active charges from the point A; the lower limit of the integration is chosen as a characteristic distance between active charges $\beta N^{-1/3}$.

Since the x component of the total field, $F_x = \sum F_{ix}$, consists of statistically independent summands, one can write its distribution function in the form of a Gaussian:

$$P_x(F_x) = (2\pi\langle F_x^2 \rangle)^{-1/2} \exp (-F_x^2/2\langle F_x^2 \rangle) . \qquad (8)$$

Changing to spherical coordinates in the $\mathbf{F}$-space, we obtain the magnitude distribution of the random electric fields:

$$P(F) = (3^{3/2}\beta^{3/2}\varepsilon^3/2^{5/2}\pi e^3 N^2)F^2 \times$$

$$\times \exp (-3F^2\varepsilon^2\beta/8\pi e^2 N^{4/3}) , \quad \beta \cong 0.18 \qquad (9)$$

The numerical parameter β was defined by equating the moment $\langle F^4 \rangle$, derived from (9), to its value obtained by summation over active charges similarly to (7).

4.2. Lifetime of the active charges — hole polarons

Positive active charges, localized on Mn^{3+} ions, form hole polarons. Their hopping within the Mn sublattice results in the disappearance of active charges via formation of coupled pairs with negative impurity ions. Below we will assume that the relaxation rate Γ of active charges through this channel is proportional to the rate of the hole polaron hopping between adjacent Mn^{3+} ions. The rate of hole hopping depends on the electric field and has a large straggling corresponding to the broad distribution (9) of the magnitude of the electric field.

Note that such an approximation can overestimate the relaxation rate of long-lived active charges after the switching off of the irradiation. Indeed, the totality of holes, in the course of their diffusive motion, rearranges to achieve a local minimum of electrostatic energy. Such a metastable configuration of holes can have a very large lifetime, significantly exceeding the characteristic time of single-hole diffusion.

Now let us consider the probability of hole hopping from the ion A, where it is localized, to another ion B. At first, the electric field is put equal to zero. If a hole remains at the ion A, the energy E_e of the electronic subsystem depends on the coordinates x_n of adjacent atoms:

$$E_e = -\sum_n C_n x_n \qquad (10)$$

(the energy is linearized in the coordinates x_n, which are counted from their equilibrium position in the absence of holes). The total energy of the crystal includes the electronic energy (10) and the lattice deformation energy, which is quadric in x_n:

$$E_{\text{tot}} = -\sum_n C_n x_n + \sum_n K_n x_n^2/2 \equiv$$

$$\equiv \frac{1}{2} \sum_n [-C_n^2/K_n + K_n(x_n - x_{0n})^2] . \qquad (11)$$

Here $x_{0n} = C_n/K_n$ is the equilibrium value of the coordinate x_n in the presence of the localized hole. Equation (11) allows to perform the high-temperature thermodynamic averaging

$$\langle (x_n - x_{0n})^2 \rangle = T/K_n \qquad (12)$$

(temperature is expressed in energy units).

To simplify the calculations, they will be carried out using Eq. (12), but the final result will be extended to the case of an arbitrary temperature.

Let a hole hop from the ion A to an equivalent ion B. At the moment of hopping the surroundings of the ion A are in equilibrium with the hole ($x_{nA} \cong x_{0n}$), but those of the ion B are the same as in the ideal lattice ($x_{nB} \cong 0$). Before hopping, the electronic energy (10) is

$$-\Delta = -\sum_n C_n x_{0n} = -\sum_n C_n^2/K_n , \qquad (13)$$

and just after hopping the electronic energy equals zero. Thus, hopping requires a fluctuation to overcome the energy gap Δ (it is just this gap which conditions the existence of stable active charges). The A-to-B hopping of the hole is promoted, to the same degree, by the fluctuations of the surroundings of both the atoms A and B. For brevity we will consider only the fluctuation around the atom A, but the final result will be written down with allowance for the fluctuations around both atoms.

The A-to-B hopping of a hole requires a fluctuation of the coordinates $x_n \equiv x_{nA}$ which turns the electronic energy (10) to zero before hopping. (Eq. (10) relates to the lattice being in equilibrium with the electronic subsystem before hopping). This condition can be presented in the form

$$\sum_n y_n = -\Delta, \; y_n \equiv (x_n - x_{0n})C_n , \qquad x_{0n} = C_n/K_n . \qquad (14)$$

The sum $y = \sum y_n$ of statistically independent coordinates has the distribution function

$$f(y) = \text{const} \exp(-y^2/2\sigma^2) . \qquad (15)$$

Using Eqs. (14) and (12), we can write the dispersion σ as

$$\sigma^2 = \sum_n \langle y_n^2 \rangle = T \sum_n C_n^2/K_n . \qquad (16)$$

The A-to-B hop of a hole becomes possible if y attains the gap $\Delta = \sum C_n^2/K_n$ between the hole

levels after and before the jump. Therefore, the hopping probability is proportional to $f(\Delta)$. In the presence of a field applied in a favorable direction, the gap is reduced by the value Fea, where a is the distance between the sites A and B. Finally, the rate of the active charge relaxation, considered to be proportional to the probability of the A-to-B hopping per unit time, can be written with allowance for (15) and (16) in the form:

$$\Gamma = \Gamma_o \exp(-\Delta/4T_{\text{eff}} + Fea/2T_{\text{eff}}) . \qquad (17)$$

Expression (17) is written in the final form, taking into account two essential details which were omitted in the course of calculations for brevity. First, the temperature T is replaced by an effective temperature T_{eff}, which coincides with T at high temperatures and allows for the zero vibrations of the lattice at low temperatures. In the Debye approximation, T_{eff} is defined as $A \langle (\mathbf{r} - \mathbf{r}_0)^2 \rangle$, where $\mathbf{r}$ is the radius-vector of an atom in the ideal lattice, $\mathbf{r}_0$ is that of the corresponding site, and the choice of the constant A provides the coincidence of T_{eff} with T at high temperatures. This definition can be rewritten in the explicit form

$$T_{\text{eff}} = (2T^2/\hbar\omega_D) \int\limits_0^{\hbar\omega_D/2T} x \coth x \, dx \qquad (18)$$

with the Debye frequency ω_D.

Second, Eq. (17) makes allowance not only for the fluctuations in the surroundings of the atom A but also for those related to the atom B (which results in the additional coefficient 2 multiplying T_{eff}).

4.3. Kinetic equation for active charges in a general form

Within the model of random electric fields developed above, the kinetic equation differs essentially from its simple form (4). The differences will be discussed in what follows.

Active charges are divided into groups, n_j, according to their lifetimes $\tau_j = \Gamma_j^{-1}$. The F axis is divided into M intervals ΔF_j (with centers at the points F_j) in a way providing equal probabilities for an arising active charge to get into every interval ΔF_j:

$$\int\limits_0^{F_j} P(F)dF = (j - 0.5)/M , \; \Delta F_j P(F_j) = 1/M, \qquad (19)$$

$$j = 1, \ldots, M$$

where $P(F)$ is the distribution function (9) for the magnitudes of the random fields. For an active charge of the jth group, the recombination rate is

$$\Gamma_j \equiv \Gamma(F_j) = \Gamma_0 \exp\left(-\Delta/4T_{\text{eff}} + F_j e a/2T_{\text{eff}}\right) . \tag{20}$$

Photoillumination supplies active charges to every of the M groups with the same probability which should be understood as follows. Light pumping transfers J electrons per unit time from Mn^{3+} ions either to Mn^{4+} ions (with a probability p) or to coupled pairs of charges (with probability $1 - p$). The total number of active positive charges is increased through the latter channel by the value $N_+ = J(1 - p)$ and decreased through the former channel by $N_- = Jp$. While the number N_+ of generated charges is uniformly distributed among the M groups, the loss N_- of charges is distributed among these groups proportionally to their populations. The probability $p = p(N)$ increases with the total number N of active charges per unit volume.

Thus one can write the kinetic equation for the populations of the M groups of active charges:

$$dn_j/dt = J\left[1/M - p(N)n_j/N\right] - \hat{\Gamma}n_j . \tag{21}$$

Here $\hat{\Gamma}$ stands for the recombination operator, which in a rough approximation can be written simply as the recombination rate Γ_j of an active charge at the moment of its generation by pumping. In fact, however, Γ varies as a function of electric field during the active charge lifetime due to random changes in the positions of other active charges (this will be allowed for in Sec. 4.4).

The kinetic equation (21) describes the experimentally observed regularities. The lifetime distribution of active charges, given by Eqs. (9) and (17), is continuous and covers a very broad range (about five orders of magnitude at $T = 100$ K and an active charge concentration of 0.1%). The kinetic equation (21) describes the saturation of the number of active charges with increasing exposition time or pumping intensity, irrespective of the relaxation by hole hopping. Indeed, in the limiting case of zero hopping rate, Eq. (21) after summation over j turns into

$$dN/dt = J[1 - p(N)] \text{ at } \Gamma_j = 0 . \tag{22}$$

As N increases, $p(N)$ grows and nears unity, so that dN/dt goes to zero. Let us introduce the characteristic value N_0 of the number of active charges at which the total growth rate is slowed down by a factor of two:

$$p(N_0) = 0.5 . \tag{23}$$

N_0 defines the scale of the saturation number of active charges under very strong pumping. Note that the characteristic number of active charges N_0 is much less than the number of inactive coupled pairs, N_{coup} :

$$N_0 << N_{\text{coup}} . \tag{24}$$

Indeed, at $N = N_0$ the total probability of electron trapping by any active charge is equal to that of electron trapping by any coupled pair. However, in the former case the trapping cross section is much larger than in the latter case due to the stronger field produced by an active charge. Hence, the total number of coupled pairs must correspondingly exceed that of active charges.

4.4. Specific form of the kinetic equation with a model description of generation and recombination of active charges

To carry out a quantitative comparison of the kinetic equation (21) with experiment, it is necessary to give concrete definitions of the recombination operator $\hat{\Gamma}$ and the probability $p(N)$ appearing in (21). In view of the highly complicated character of the corresponding physical processes, this will be done below in a model way.

At the moment of its generation, an active charge of the jth group has the recombination rate (20) determined by the random field value F_j . After that, the recombination rate of this charge varies due to electric field variations caused by the disappearance and generation of other active charges at random points. The random field F and the corresponding recombination rate of a given active charge are changed substantially when a significant fraction of the other active charges is replaced by new generated charges. The fraction of new active charges, generated during the time dt, is $Jdt/N(t)$. This quantity, integrated over time, can serve as a measure of the corresponding change in the argument of Γ_j . Within the model, this is allowed for through a shift in the argument of the monotonically growing sequence Γ_j ($j = 1, \ldots, M$):

$$\hat{\Gamma}n_j = n_j\Gamma_{j + Ms} , \quad s(t) = \int_0^t Jdt/N(t) \tag{25}$$

(the definition of Γ_j in Eq. (20) is periodically extended over the infinite interval j with the period M). The lower limit of integration in (25) does not play any role: a constant addition to $s(t)$ only

redefines the numbering of the active charge groups, which has no physical consequences.

Now let us consider the probability p for an electron, removed by pumping from a Mn^{3+} ion, to be captured by one of the positive active charges (the alternative possibility is its capture by one of the inactive coupled pairs). Let us assume that an electron is captured by an active charge under the condition

$$F_{act} \equiv 1/\varepsilon r^2 > F_{bac} \qquad (26)$$

where F_{act} is the electric field of an active charge at the distance r and F_{bac} is the characteristic magnitude of the background field of coupled pairs (according to (24), their number greatly exceeds the number of active charges). F_{bac}^2 can be estimated as the squared field of the dipole $\mathbf{d}$, $F_0^2 = 2d^2/R^6\varepsilon^2$, averaged over its orientations ($R = N_{coup}^{-1/3}$ is the mean distance between the dipoles). The quantity F_0^2 should be multiplied by the actual number Z of dipoles with the moment $d = ea$, where a is the lattice constant. (Below we set $Z = 12$ as for a close-packed lattice). Thus the condition (26) of electron trapping by an active charge takes the form

$$r < r_0 , \qquad r_0 \equiv (24)^{-1/4}(aN_{coup})^{-1/2} . \quad (27)$$

The condition (27) is not met only if *none* of the NV active charges, randomly situated in the crystal volume V, is found inside the spherical volume $V_0 = (4/3)\,\pi r_0^3 << V$. The probability for *one* active charge to be found outside the sphere is $1 - V_0/V$; for NV charges this quantity should be raised to the power NV, resulting in $\exp(-NV_0)$. Thus, the probability for the condition (27) to be fulfilled is

$$p(N) = 1 - \exp(-NV_0) = 1 - \exp[-(4/3)\pi Nr_0^3] , \qquad (28)$$

where r_0 is defined by Eq. (27).

We would like to remark that the probability $p(N)$ could be defined in some other model way; however, the calculations show that this would not exert any noticeable effect on the solution of the kinetic equation.

According to the definition (23), the characteristic number of active charges per unit volume is

$$N_0 = 1.8(aN_{coup})^{3/2} . \qquad (29)$$

Note that this relation meets the inequality (24).

To simplify the form of the kinetic equation (21), let us introduce the number ν of active charges expressed in units of N_0 :

$$\nu = N/N_0 , \; \nu_j = n_j/N_0 , \; \nu = \sum_j \nu_j . \quad (30)$$

Now the kinetic equation takes the form

$$dv_j/dt = I[\frac{1}{M} - (1 - 2^{-\nu})\nu_j/\nu] - \nu_j\Gamma_{j+Ms(t)} ,$$

$$s(t) \equiv \int_0^t I\,dt/\nu(t) \qquad (31)$$

where I is the pumping intensity in some units. (I is proportional to the experimental pumping intensity i).

5. Photoinduced absorption. Comparison of the theory with experiment

The problem under consideration is specified by the following physical parameters:

(i) The number a^3N_{coup} of negative impurity ions, which form coupled pairs of charges in the ground state, per unit cell. The corresponding number of active charges per unit cell is $1.8\nu \times \times (a^3N_{coup})^{3/2}$. These parameters specify the distribution function (9) of the electric fields.

(ii) The depth Δ of the deformation potential well of a Mn-hole polaron.

(iii) The Debye frequency ω_D , which specifies the effective temperature (18) and together with the parameters Δ and Γ_0 determines the recombination rate (17) as a function of temperature.

(iv) The proportionality coefficient between N and ΔK and that between I and the experimental pumping intensity i are chosen as fitting parameters.

The solution of the kinetic equation (31) is fitted best to the entirety of experimental data for the following set of parameters: $\Delta = 1.08$ eV = 12500 K; $\hbar\omega_D = 0.035$ eV = 400 K; $\Gamma_0 = 7 \cdot 10^5$ s^{-1}. The characteristic number N_0a^3 of active centers per unit cell is equal to 0.2%, and the number of active centers achieved under full pumping ($i = 1$), amounts to 0.08%. The corresponding number of coupled pairs of charges per unit cell is 1%.

These values of the parameters seem reasonable for a solid. In particular, active charges of the given concentration create an electric field of about $1.5 \cdot 10^6$ V/cm, which is roughly 300 times less than the intra-atomic field. This leads to an oscillator strength of about 10^{-5} for a forbidden transition. In

the visible range this corresponds to an absorption coefficient of the order of 100 cm^{-1}, which is in qualitative agreement with experiment. The rather large depth of the polaronic potential well ($\Delta = 1.08$ eV) is associated with the Jahn−Teller lattice deformation changing during the Mn-hole hopping.

Let us compare the solution of the kinetic equation (31), obtained for this set of parameters, with the experimental data. In Figs. 4, 5, 7 the solid lines show the calculated augmentation of the absorption coefficient, ΔK, produced and measured with unpolarized light. The figures demonstrate a qualitative agreement of the theory with the experiment within broad ranges of temperature and pumping intensity, both under irradiation with light and after the pumping is switched off.

In the latter case, the calculated relaxation rate of the total photoinduced absorption (solid lines in Fig. 5) systematically exceeds the experimental one. To all appearance, this discrepancy originates from multiparticle phenomena (mentioned at the beginning of Sec. 4.2) which have not been taken into account in the above theory.

Attention should be drawn also to another discrepancy between the theory and experiment shown in Fig. 5. In the basic assumptions (Sec. 1, Item 4) and in the theory, the response of the crystal to pumping is described by one characteristic time. Such a description, however, is not quite exact. As can be seen from Fig. 5, the experimental time dependences of photoinduced absorption under pumping, measured at various temperatures, exhibit at least two characteristic times t_1 and $t_2 \gg t_1$. At first, the absorption grows fast during the time $t_1 \cong 2$ min, but this fast growth stops at the level $\Delta K(\infty) - K_1$ near the complete saturation level $\Delta K(\infty)$ ($K_1 \ll \Delta K(\infty)$). After that, the absorption reaches complete saturation much more slowly, with the characteristic time $t_2 \cong 10$ min.

The theory developed above describes the fast process only. The slow process can be associated with deep hole traps (probably Mn^{3+} ions located in the vicinity of some lattice defects). Initially the traps are empty and neutral, but after filling by holes they begin to act as stable active charges with an infinite recombination time τ (a pinned hole cannot recombine with a pinned negative charge). At low temperatures, the contribution of trapped holes to the photoinduced absorption amounts to about 10%; hence, their concentration is ten times less than the total concentration of active charges and amounts to $c_{tr} \cong 2 \cdot 10^{-4}$. Due to their low con-

centration, the traps are filled slowly, which explains the large characteristic time t_2.

The contribution of filled traps to the absorption, presented in Fig. 5 by the experimental curves, can be satisfactorily described in the exponential form

$$\Delta K_{tr}(t) = K_1 \left[1 - \exp\left(- t/t_2\right) \right], \qquad (32)$$

with parameters that are almost constant in the temperature range $T \leq 100$ K: $K_1 \cong 10$ cm^{-1} and $t_2 \cong 7$ min. At $T = T_1 = 130$ K, K_1 diminishes by roughly a factor of two. This allows us to estimate the trap depth as $T_1 \ln\left(1/c_{tr}\right) \cong 1100$ K $= 0.1$ eV.

6. Photoinduced dichroism: Additional information on electronic processes

As was already noted, photoinduced dichroism and birefringence are of the same nature: they display quite similar temperature dependences and relaxation curves after the switching off of the irradiation. Earlier [13], the observed dependence of birefringence on the pumping polarization direction was described with taking into account the crystallographic structure of the Ca$_3$Mn$_2$Ge$_3$O$_{12}$ garnet. Below, this mechanism is generalized somewhat to include birefringence and dichroism simultaneously.

The surroundings of each Mn^{3+} ion have the symmetry of a distorted octahedron. This distortion eliminates the degeneracy of the angular 3d states of the Mn-hole localized at the center of the octahedron. For brevity, the polarization axis of the hole state with the minimal energy will be called the octahedron axis (it may coincide, for example, with the tetragonal axis along which the octahedron is contracted due to the Jahn−Teller deformation of the lattice; note that the energy scale of the Jahn−Teller effect exceeds that of the temperature within the temperature region examined). At low temperatures, all the occupied hole states are polarized along the octahedron axes. The total set of octahedrons can be divided into chains in such a way that octahedron axes have nearly the same direction within the same chain, but the axis directions differ strongly for chains of different types.

The direction of the pumping light polarization dictates the predominant polarization of generated holes, i.e., the type of chains predominantly occupied by holes. Thus a polarized pumping induces anisotropy of the optical properties, which manifests itself both in birefringence and in dichroism.

It can be seen from Fig. 10 that the relaxation curves of photoinduced dichroism and birefringence

practically coincide with the relaxation curve of the photoinduced absorption. This means that after the switching off of the irradiation, the hole polarization and the active charge itself relax in the same way: the initial polarization direction persists until the hole forms a coupled pair with a negative impurity. In other words, a hole retains its polarization direction when hopping between adjacent Mn ions.

Based on this, the relaxation process can be generally described as follows. After the illumination is switched off, a hole hops within the same chain until recombination with a negative impurity charge occurs. The probability for a hole to meet an impurity charge just in the same chain is negligibly small. However, a hole can leave the chain in the strong field of a negative charge lying near the chain, thus changing its polarization and simultaneously disappearing as an active charge (forming an inactive coupled pair).

Now let us draw attention to the different temperature dependences of the photoinduced dichroism (Fig. 11) and absorption (Fig. 7, upper curve) measured under pumping after saturation. This difference suggests that pumping modifies the relaxation process somewhat. During relaxation without pumping, as was mentioned in Sec. 4.2, the totality of active charges is rapidly rearranged to minimize their electrostatic energy; because of this the random electric fields are weak and insufficient to force a hole to leave its chain. However, pumping rapidly changes the configuration of active charges and strongly enhances the straggling of their fields. In the course of relaxation *under pumping*, a hole can find itself in a strong random field, which causes it to leave the chain and to change polarization even far from negative impurities. Thus, pumping gives rise to a new relaxation channel which affects only the dichroism. This can explain the observed distinction of its temperature dependence under pumping from that of the photoinduced absorption.

In more detail, this distinction can be understood under the assumption that the two types of hole motion — hopping within the same chain and hopping between different chains in a strong field — are associated with different sets of lattice vibrations. In Sec. 4.2, the relaxation of active charges (i.e., hole hopping within a chain) was satisfactorily described in the Debye approximation which involves the total set of frequences. Low-frequency vibrations from this set are responsible for a decrease of photoinduced absorption with increasing temperature, both with and without pumping. To

all appearances, hole hopping between different chains is associated with a set of sufficiently high frequencies. The amplitudes of such vibrations begin to increase with temperature only above 100 K, which explains the rather weak temperature dependence of the dichroism measured under pumping (supposing that dichroism relaxes mainly through hopping between chains). In the absence of pumping, this relaxation channel is inactive, and dichroism relaxes only through hopping within the same chain (associated with low-frequency vibrations of the lattice). This explains the noticeable temperature dependence of the relaxation rate in the total interval of temperatures, observed in the absence of pumping for the dichroism and birefringence (as well as for photoinduced absorption).

Conclusion

Experiments performed with the garnet $Ca_3Mn_2Ge_3O_{12}$ display unusual features of the photoinduced absorption:

saturation of the photoinduced absorption with pumping intensity;

a broad distribution of photoinduced absorption centers over relaxation times, with the predominance of very long times;

the coincidence of the relaxation rates of photoinduced absorption and dichroism and a noticeable difference between their temperature dependences under pumping.

Such experimental results cannot be understood in terms of photoinduced absorption centers associated with impurities or lattice defects. Within the notion of random electric fields, a quite natural explanation can be given: the Mn^{3+} sublattice of the $Ca_3Mn_2Ge_3O_{12}$ garnet contains Mn^{4+} ions (i.e., Mn-holes) in a low concentration [19,20]. As the crystal as a whole must be electrically neutral, it contains negative impurity ions or cation vacancies in the corresponding concentration. In the ground state, the Mn-holes occupy Mn sites adjacent to negative impurity charges. Such coupled pairs of opposite charges are inactive in the sense that their electric field is very weak in the major part of the crystal volume.

Under photoillumination, a small number of electrons are transferred from regular Mn^{3+} ions to the Mn^{4+} components of coupled pairs, thus creating pairs of spatially separated charges of opposite signs (active charges). Active charges create electric fields in a larger volume than coupled pairs and correspondingly enhance the probability of the forbidden optical transition. At low concentrations of active charges, the photoinduced absorption is pro-

portional to it. Photoinduced dichroism is caused by the predominant generation of holes polarized in a fixed direction. They are responsible for an anisotropic distortion of their surroundings which entails dichroism and birefringence (their time and temperature dependences are quite similar).

The random electric fields of active charges simultaneously manifest themselves in another way: they promote the relaxation of photoinduced changes through hopping of holes. A broad distribution of the magnitudes of the random fields gives rise to a very broad range of hole hopping rates and, hence, of the lifetimes of the photoinduced changes.

Simultaneously, the existing active charges annihilate during the photoproduction of new active charges: electrons, removed from Mn^{3+} ions by pumping, are also transferred to active charges (Mn^{4+} ions). The characteristic time of this annihilation channel is inversely proportional to the pumping intensity. Under an increase of the pumping intensity this relaxation channel becomes predominant, which results in the saturation of photoinduced changes with pumping.

Photoinduced dichroism and birefringence display the same temperature dependence under pumping and the same time dependence after switching off the irradiation. This provides evidence for a similar nature of photoinduced dichroism and birefringence: they are caused by the anisotropic distribution of Mn-holes, created by polarized pumping, over the polarization directions. The coincidence of the relaxation curves of the photoinduced absorption and dichroism can be seen as a hint that Mn-holes retain their polarization direction when hopping; this can be explained by taking into account some structural features of the $Ca_3Mn_2Ge_3O_{12}$ garnet.

Acknowledgements

1. R. W. Teale and D. W. Temple, *Phys. Rev. Lett.* **19**, 904 (1967).
2. R. F. Pearson, A. D. Annis, and P. Kompfner, *Phys. Rev. Lett.* **21**, 1805 (1968).
3. J. F. Dillon, E. M. Gyorgy, and J. P. Remeika, *Phys. Rev. Lett.* **23**, 643 (1969).
4. V. F. Kovalenko, E. S. Kolezhuk, and P. S. Kuts, *Zh. Eksp. Teor. Fiz.* **81**, 1399 (1981) [*Sov. Phys. JETP* **54**, 742 (1981)].
5. K. Hisatake, K. Ohta, N. Ichinose, and H. Yokoyama, *Phys. Status Solidi* **A26**, K75 (1974).
6. M. Pardavi-Horvath, P. E. Wigen, and G. Vertesy, *J. Appl. Phys.* **63**, 3110 (1988).
7. H. Van der Heide and U. Enz, *Solid State Commun.* **6**, 347 (1968).
8. W. Lems, R. Metselaar, P. J. Rijnierse, and U. Enz, *J. Appl. Phys.* **41**, 1248 (1970).
9. V. G. Veselago, N. V. Vorob'ev, and R. D. Doroshenko, *Pis'ma v ZhETF* **45**, 402 (1987) [*JETP Lett.* **45**, 512 (1987)].
10. E. M. Gyorgy, J. F. Dillon, and J. P. Remeika, *J. Appl. Phys.* **42**, 1454 (1971).
11. K. Hisatake, I. Matsubara, K. Maeda, H. Yasuoka, H. Mazaki, and K. Vematsu, *J. Magn. Magn. Mater.* **140–144**, 2127 (1995).
12. V. A. Bedarev, S. L. Gnatchenko, R. A. Rupp, and B. Sugg, *Fiz. Nizk. Temp.* **24**, 281 (1998) [*Low Temp. Phys.* **24**, 212 (1998)].
13. S. L. Gnatchenko, V. V. Eremenko, S. V. Sofroneev, and N. F. Kharchenko, *Pis'ma v Zh. Eksp. Teor. Fiz.* **38**, 198 (1983) [*JETP Lett.* **38**, 233 (1983)].
14. S. L. Gnatchenko, N. F. Kharchenko, V. A. Bedarev, V. V. Eremenko, M. Artinian, J.-M. Desvignes, and H. Le Gall, *Fiz. Nizk. Temp.* **15**, 627 (1989) [*Sov. J. Low Temp. Phys.* **15**, 353 (1989)].
15. V. A. Bedarev and S. L. Gnatchenko, *Fiz. Nizk. Temp.* **20**, 124 (1994) [*Low Temp. Phys.* **20**, 100 (1994)].
16. B. Sugg, S. L. Gnatchenko, and R. A. Rupp, *J. Opt. Soc. Am.* **B13** 2662 (1996).
17. R. Alben, E. M. Gyorgy, J. F. Dillon, and J. P. Remeika, *Phys. Rev.* **B5**, 2560 (1972).
18. M. Wurlitzer and J. Franke, *Phys. Status Solidi* **A64**, 539 (1981).
19. A. E. Nosenko, B. V. Padlyak, and V. V. Kravchishin, *Fiz. Tverd. Tela* **27**, 3455 (1985).
20. B. V. Padlyak, and A. E. Nosenko, *Fiz. Tverd. Tela* **30**, 1788 (1988).
21. Z. A. Kazei, P. Novak, and V. I. Sokolov, *Zh. Eksp. Teor. Fiz.* **83**, 1483 (1982) [*Sov. Phys. JETP* **56**, 854 (1982)].
22. S. L. Gnatchenko, V. V. Eremenko, S. V. Sofroneev, N. F. Kharchenko, J.-M. Desvignes, P. Feldmann, and H. Le Gall, *Zh. Eksp. Teor. Fiz.* **90**, 179 (1986) [*Sov. Phys. JETP* **63**, 102 (1986)].
23. W. Graeff, J. Kub, and K. Wieteska, *Phys. Status Solidi* **A126**, 477 (1991).
24. L. E. Orgel, *J. Chem. Phys.* **23**, 1004 (1955).
25. R. Pappalardo, *Philos. Mag.* **2**, 1397 (1957).